

## Sononanoengineered magnesium–polypyrrole hybrid capsules with synergetic trigger release

Ekateriva V. Skorb,<sup>\*a</sup> Olga Baidukova,<sup>a</sup> Ankit Goyal,<sup>a</sup> Adam Brotschie,<sup>a</sup> Daria V. Andreeva<sup>b</sup> and Helmuth Möhwald<sup>a</sup>

Received 8th February 2012, Accepted 24th April 2012

DOI: 10.1039/c2jm30768e

This paper describes the ultrasonic-assisted preparation and characterisation of magnesium–polypyrrole hybrid capsules loaded with the organic fluorophore rhodamine 6G (Rh6G). Hybrids were prepared through sonication of magnesium and pyrrole without initiator or with Fe(III) as the polymerisation initiator in water and alcohol solutions. We studied the hybrids' morphology,  $\zeta$ -potential, FTIR spectra, sonoinduced phase transformation and fluorescent properties. The properties of the obtained hybrids, as well as the dye-loading efficiency, were found to depend on the ultrasonic conditions. The fluorophore release from the free or surface sonoimmobilised capsules in aqueous solutions of different pH values and under electric current was also studied. Effective pH-responsive release, including step-wise release, was confirmed for the hybrid system. The electric current was also shown to trigger the release of hybrid capsules sonoimmobilised onto an Ni patterned ITO surface.

## Introduction

Conducting polymers like polypyrrole have attracted great attention due to their conductive nature, good adhesion properties onto metal surfaces, anticorrosive nature and stability under harsh environmental conditions.<sup>1–3</sup> Polypyrrole (Ppy) finds vast applications in anticorrosive coatings,<sup>1</sup> biosensors,<sup>4</sup> controlled drug delivery,<sup>5</sup> gas sensors,<sup>6</sup> photovoltaic cells,<sup>7</sup> fuel cells,<sup>8</sup> artificial muscles,<sup>9</sup> *etc.* There are several methods for pyrrole polymerisation, for example using oxidants like ferric salts,<sup>10</sup> ammonium persulfate<sup>11</sup> or using cationic photoinitiators like iron arene salts,<sup>12</sup> *etc.* For biological applications, polypyrrole has advantages as it is biocompatible, stable and conductive.<sup>13</sup> Its conductive nature allows an applied current to be switched on and off reversibly, to facilitate the controlled delivery of drugs or release of other chemicals. In addition, due to its stability, it can protect the capsules used in controlled release systems from degradation before reaching the target site. These properties of Ppy help to overcome the present problem of achieving efficient low molecular weight active component delivery.

Various nanoparticles, such as Fe<sub>2</sub>O<sub>3</sub>, Ag, Pd, Au, Ti, TiO<sub>2</sub>, V<sub>2</sub>O<sub>5</sub> and C, have been used to form Ppy nanocomposites.<sup>3,14,15</sup> There has been to date, however, no reported study of reactive templating, for example, with calcium carbonate or, as presented

in this paper, active metals (Mg). One should take into account that comparing the conductivity, magnesium has lower conductivity than noble metals such as Au or Ag. However, magnesium is very interesting as a templating material due to its biocompatibility, degradability and possible application as an *in vivo* corrosion implant.<sup>16,17</sup> Moreover, it was shown by us recently that magnesium (also Al, but not Au or Ag) could be effectively converted into sponges by application of ultrasound even in pure water. We have investigated several groups of metals under different sonication conditions. Magnesium chosen for this study is ideal as it is liable to undergo oxidation and its melting point is within the range achievable during ultrasonic processes (cavitation and inter-particle collisions). This simple process, free of byproducts, also enables the loading of sponges with active agents in the same process. The sponges system can be loaded with active chemicals (vitamins and drugs, corrosion inhibitors, enzymes, DNA fragments, antibodies, bone morphogenetic proteins, *etc.*). As an analogue to novel Mg sponges, a drug carrier providing time-controlled drug release on demand that is widely applied nowadays is CaCO<sub>3</sub>.<sup>18</sup> A pH change could be used as an appropriate trigger to control release in the case of magnesium and magnesium-based hybrids. One of the great advantages of the Mg–Ppy hybrid, compared with Mg itself, is the possibility of construction of a unique encapsulation system, having porous surfaces with active component release on demand.

In the present work we describe an ultrasound-assisted method for the formation of magnesium–polypyrrole hybrid capsules with and without an initiator (Fe(III)). Ultrasound has many advantages over conventional synthesis techniques because it is

<sup>a</sup>Max Planck Institute of Colloids and Interfaces, Wissenschaftspark Golm, Am Mühlenberg 1, 14476 Golm, Germany. E-mail: skorb@mpikg.mpg.de; Fax: +49 331567 9202; Tel: +49 331567 9233

<sup>b</sup>Physical Chemistry II, University of Bayreuth, Universitätsstr., 30, Bayreuth, 95440, Germany

both environmentally friendly and cheap. Reactions that with other techniques would require the use of harsh reaction conditions (high temperature, high pressure and in organic solvents) can be carried out in aqueous systems under ambient conditions with ultrasound.<sup>19–22</sup> Not only does this allow reactions to be carried out under milder conditions but it also reduces the number of synthesis steps, permits the use of lower purity chemicals and gives higher yields.<sup>23</sup> Moreover, for polymerisation reactions, ultrasound can increase the reaction rate and monomer conversion percentage, compared with other techniques, largely because it enhances mass transport to the reaction site.<sup>24</sup> In particular, the molecular weight of Ppy in the hybrid system can depend on temperature, pressure, gas content, pH, solvent, duration and intensity of the ultrasound. Moreover, in the case of hybrid systems, of great importance is the matrix (here Mg) and its response to ultrasound as well as porosity type (pore shape and size). Despite great interest<sup>25–27</sup> in the prospective field of metal–polymer interactions due to the application of high-intensity ultrasound (thought to arise through cavitation-assisted processes), there is still a general lack of knowledge about such processes. A few reports have concentrated on characterisation of the chemical interactions between metals and untreated polymer surfaces, whereas some others have concentrated on plasma-treated polymer surfaces. From the studies on untreated polymer surfaces, several general observations can be made. Typically, for polymers that do not contain carbon–oxygen or carbon–nitrogen functionalities, little to no chemical interaction is observed, irrespective of the reactivity of the metal.<sup>28</sup> For reactive metals, such as Al, Mg, Cr, and Ni, extensive chemical interactions can occur, typically with oxygen atoms in oxygen-containing polymers.<sup>29</sup> For metals with moderate chemical reactivity, such as Cu, Ti and Ag, chemical interactions were found to be polymer dependent.<sup>30</sup> The formation of defined hybrids using the green ultrasonic method is of great interest due to their advanced functionalities (*e.g.*, synergetic (pH and electric current) time-resolved active component release), which can be used as capsules.

Rhodamine 6G (Rh6G) is a cationic lipophilic dye, which is among the most stable organic fluorophores. It is mostly applied in laser technology, as well as having applications in fluorescent bio-imaging.<sup>31–33</sup> Owing to its lipophilic character, Rh6G is also known as a distinct stain for lipids and phospholipid-based polymers.<sup>32</sup> Systems loaded with the Rh6G fluorophore may be useful for different biological and technological applications. For example, polymer particles incorporating dyes are applicable to cell labelling,<sup>33</sup> sensitive diagnostic reagents,<sup>34</sup> flow tracing<sup>35</sup> and electronic inks.<sup>36</sup> Thus, in this work we chose Rh6G as a model to investigate novel hybrid materials formed through sonication for low molecular weight molecule storage and release on demand.

## Experimental section

### Materials

Magnesium particles used for the experiments were supplied by Alfa Aesar of -325 mesh size and 99.8% purity and were used as received. Pyrrole (98%, reagent grade) was supplied by Sigma Aldrich. For all experiments, water was purified before use in a three-stage Millipore Milli-Q Plus 185 purification system and

had a conductivity lower than 18.2 MΩ cm. Fe(III) (FeCl<sub>3</sub>·6H<sub>2</sub>O, 97% purity, Sigma Aldrich) was used as the pyrrole polymerisation initiator. Rhodamine 6G (Rh6G) was supplied by Sigma Aldrich and had a 98% dye content.

### Magnesium PPy hybrid preparation

Magnesium powder was sonicated in 60 mL Milli-Q water or alcohol solution with a 20 kHz horn-type sonicator (Hielscher UIP1000hd, Germany) equipped with a booster B2-1.2, operated with a maximal output power of 1000 W. The surface area of the horn tip (Hielscher, BS2d22) was 3.8 cm<sup>2</sup> and sonication was performed in a thermostatted flow cell (FC100L1-1S) at 65 °C. The maximum calorimetric intensity was calculated as 57 W cm<sup>-2</sup> at a mechanical amplitude of 81 μm. Samples were centrifuged after sonication and then dried after removing the extra water.

### Experiments with pyrrole without initiators

Magnesium particles were sonicated in solution for 5 minutes. Pyrrole was subsequently added to achieve 5 wt% pyrrole solution and sonication was continued up to 30 minutes. The weight ratio of magnesium : pyrrole was 2 : 1.<sup>37</sup>

### Experiments with initiators

Fe(III) was used as the initiator. The molar ratio of iron : pyrrole was 3.4 : 1. We sonicated magnesium with aqueous salt solution for 5 minutes and then pyrrole was added as described above.

### R6G loading

Samples were loaded by simultaneous sonication of magnesium and Rh6G. Thus magnesium was sonicated for 5 minutes in the presence of Rh6G. Pyrrole was then added and sonicated as described above.

### Capsule sonoimmobilisation

An ITO glass metal patterned surface was formed as in ref. 38–40 and placed in a home-manufactured Teflon sample holder that allowed the sample to be held at a reproducible distance from the ultrasonic horn. This sample holder allowed a flat angle treatment of the sample with a 2 cm distance between the probe and the sample. Preformed hybrid capsules (10 wt%) were added to an aqueous solution and sonicated for 5 minutes under the same conditions as above. The glass containing the sonoimmobilised hybrid capsules was then washed several times and dried in N<sub>2</sub> flow.

### Characterization

A Zeta Sizer Nano ZS (Malvern Instruments, UK) was used to determine the size distribution and ζ-potential of the containers.

### Microscopy

A conventional transmission electron microscope (TEM), a Zeiss EM 912 Omega (Carl Zeiss AG, Germany), equipped with an electron diffraction unit was used. It was operated at 120 kV and was employed to study the particles' morphology, crystal structure and local orientation. Scanning electron microscopy (SEM)

was performed with a Gemini Leo 1550 instrument at an operating voltage of 3 keV to study the morphology of the samples. A Leica TCS SP (Leica, Germany) confocal laser scanning microscope (CSFM) with a 100 $\times$  oil immersion objective and numerical aperture of 1.4 was also used.

### Infrared spectroscopy

Fourier transform infrared (FTIR) measurements were carried out with a Bruker Hyperion 2000 IR microscope equipped with a 158 IR objective and MCT detector, operated at room temperature with KBr pellets. For powdered samples the traditional infrared analysis method is the collection of a KBr pellet spectrum with an aliquot of the sample. Spectra between 400 and 4000  $\text{cm}^{-1}$  were recorded with 2  $\text{cm}^{-1}$  resolution in the transmission mode using a DTGS detector.

### X-ray diffraction

XRD patterns for phase identification were collected using a Bruker D8 diffractometer with  $\text{CuK}\alpha$  radiation ( $\lambda_1 = 1.54053 \text{ \AA}$ ). Data were measured over the range of  $2\theta = 5$  to  $90^\circ$ , at steps of  $0.05^\circ$  and 1.0 s per step.

### Nitrogen sorption

Nitrogen adsorption–desorption isotherms were measured at 77 K using a Quantachrome Quadrasorb adsorption instrument and the BET method was used for surface area determination.

### Cavitation bubble dynamics

Bubble oscillation and collapse dynamics were investigated by measuring the intensity of scattered laser light from a spatially stable single bubble.<sup>41</sup> A rectangular glass resonator cell was constructed with a piezo-ceramic transducer glued to the base. Degassed water (24 mbar, 105 mL) was added to the cell, which was subsequently tuned to resonance (27 kHz) using a power amplifier (Krohn-Hite, model 7500) and function generator (Linear Krohn-Hite, model 1200A). With the acoustic pressure initially set at 0.9 bar (measured with a Dapco Industries needle hydrophone), a bubble was introduced to the solution by dropping water on the air–water surface with a syringe. The bubble forms at the acoustic pressure antinode of the cell, where it is spatially stable for several minutes. A 5 mW pen laser was aligned with the bubble and an end-on Hamamatsu photomultiplier tube was orientated at 90 degrees to the laser beam. The scattered light intensity from the oscillating bubble was then captured on a digital oscilloscope (Hameg, model HM407), which was connected to a PC. Using the same solution and experimental conditions, pyrrole was added and the experiment repeated. This procedure was then performed at a higher acoustic pressure of 1.1 bar, in order to observe the influence of the additive on sonoluminescence (emitted from the bubble in water above a threshold pressure of about 1 bar).

### Release experiments

The loading efficiency was determined *via* absorption (8453 UV-visible spectrophotometer, Agilent Technologies) and

fluorescence (FluoroMax-4, HORIBA Jobin Yvon) techniques. The hybrid capsules were dispersed in water. The dispersion was stirred for a chosen time and then centrifuged. The supernatant was then filtered to remove the remaining particles. As a reference, water solutions of the respective Rh6G with known concentrations were prepared and a calibration curve was recorded. A fluorimeter (FluoroMax-4) was used to determine the release dynamics in water. A water suspension of hybrid capsules ( $0.02\text{--}0.05 \text{ mg mL}^{-1}$ ) was placed in a quartz cuvette. The fluorescence intensity was observed every 2 minutes and the scattering was suppressed by polarising filters in the excitation and detection beams. The optical density at the absorption bands of highest wavelength was set below 0.1 to avoid reabsorption effects. Different pH regions were analysed. Absorption was also measured after step-wise changing of the pH. The electric current-induced release from sonoimmobilised capsules was studied *in situ* in confocal fluorescence mode.

## Results and discussions

There has been emerging interest in the last few decades in hierarchically ordered 3-D networks, which can be considered as carriers for active chemicals.<sup>42–44</sup> Green and inexpensive production of such carriers is a major focus of current research, as is their formation and well-defined organisation to achieve controllable chemical release. The application of ultrasound for metal-based sponge formation due to metal modification has been the focus of our work over the last two years.<sup>21,23,33,45–48</sup> We have demonstrated that these sponges may be used as carriers of active chemicals. The general concept of ultrasound-driven modification of metal microparticles ( $\mu\text{Ps}$ ) in water is as follows: the mechanism of modification of the metal structure under ultrasound irradiation is complex and involves a variety of aspects related to thermal etching and oxidation of metal surfaces. It is seen from Fig. 1 that modification of magnesium proceeds through different stages, and at the end we can achieve a total transformation of the metal to brucide (Fig. 1f).

For chemical carriers, the most important structure is one with maximal porosity, which in our case is achieved for the partially oxidised mesoporous magnesium  $\mu\text{Ps}$  (Fig. 1b and 2). The same

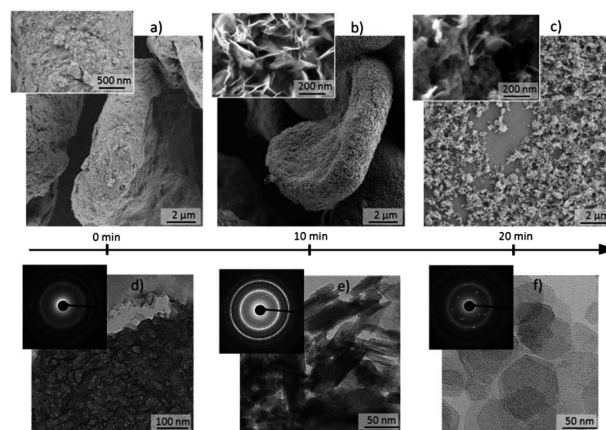


**Fig. 1** Influence of sonication time on magnesium particles: (a–c) SEM and (d–f) TEM/ED images of initial, 10 minutes and 20 minutes sonicated samples.

tendency of crystalline phase sonotransformation was shown for aluminum,<sup>21</sup> with one possible phase being a mesoporous metal skeleton stabilised with an oxidised metal nanolayer. It was shown that the surface areas for the same sonication time for Mg and Al were  $69 \text{ m}^2 \text{ g}^{-1}$  and  $54 \text{ m}^2 \text{ g}^{-1}$ , respectively. Furthermore, Mg sponges were characterised by larger pores than Al sponges: the average pore diameters were about 14 nm in the case of Mg and about 4 nm in the case of Al.<sup>21</sup> The modification of magnesium is faster in comparison with aluminum and, therefore, in the present study we use a shorter sonication time in comparison with that in ref. 21, trying to prevent total structure oxidation in favour of achieving higher porosity. Indeed, as is evident in Fig. 3, we achieve an even more porous structure with a surface area of  $260 \text{ m}^2 \text{ g}^{-1}$  and pore size of 7 nm.

Development of hybrid capsules is suggested for a system of three components: liquid (water or alcohol); solid (Mg- $\mu$ Ps); and a chosen additive (pyrrole) (Fig. 3).

The most pronounced effects of ultrasound on liquid–solid systems are both mechanical and chemical, attributed to symmetric and asymmetric cavitation collapse and active species formation in the reaction medium (Fig. 3). Symmetric bubble collapse in a liquid medium causes shock waves with high pressures in addition to high gas temperatures in the collapsed cavities. These high-pressure, high-temperature conditions exist for short time periods and are unique for the synthesis of complex hybrids with the reactor at ambient conditions.<sup>19–22</sup> Shock waves also potentially create microscopic turbulences.<sup>49</sup> This phenomenon increases the transfer of mass across the solid, thus increasing the intrinsic mass-transfer coefficient, as well as possibly creating or modifying existing 3-D networks, such as hybrid solid (Mg)–polymer (Ppy formed from pyrrole) interactions. Alternatively, this phenomenon may result in further and/or different 3-D ordering of the network formed. When bubble collapses occur near a solid surface that is several orders of magnitude greater in scale than the cavitation bubbles,<sup>50</sup> they occur asymmetrically,<sup>51</sup> and solvent microjets are formed perpendicular to the solid surface. These microjets have an estimated speed of  $100 \text{ m s}^{-1}$  (ref. 19) and lead to pitting, erosion of the surface, particle breakage and collision. Moreover, this behaviour leads to an enhancement in heterogeneous reactions (secondary cavitation-assisted processes) with active species formed in the reactor. Thus, a part of the vaporised molecules from the surrounding medium can be dissociated to form radical species, such as OH and H, for water sonolysis.<sup>52</sup> Radicals can also form by hydrogen abstraction of some organic additives

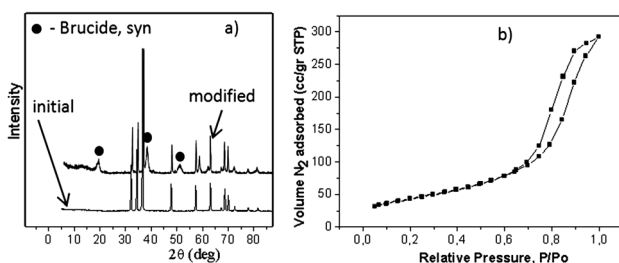


**Fig. 2** (a) XRD patterns of initial (upper) and modified (lower) (10 minutes sonication) magnesium particles; (b)  $\text{N}_2$  adsorption–desorption of modified magnesium particles.

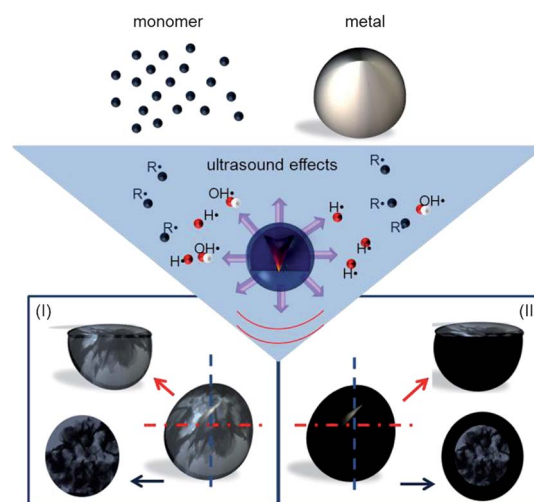


**Fig. 3** Schematic representation of the research objectives and sonochemical synthesis mechanism: initial materials – monomer, metal (magnesium)  $\mu$ Ps – upper part; possible ultrasonic effects in the reactor – physical (shock waves and liquid jets) and chemical (formation of radicals from monomer and sonolysis of the liquid vapour (here, water shown)) – middle part; and some examples of systems which could be expected after applying ultrasonic exposure: the metal and polymer could form a porous hybrid system; formation of core@shell structures such as metal and/or hybrid@polypyrrole – lower part of the scheme.

(e.g., RH forms R), either by reaction with a primary radical formed during cavitation collapse and/or by the direct pyrolysis of RH molecules during bubble collapse.<sup>53</sup> Recent studies<sup>21,23,27,45–48,54</sup> have suggested scenarios and provided prospective defined cavitation pathways for surface modifications based on the surfaces' different responses to ultrasound. The different responses result from differences in the surfaces' hydrophilic/hydrophobic properties or chemical reactivity. Thus, comparison of bubble formation on hydrophobic and hydrophilic surfaces with that in the bulk reveals a stronger response on the hydrophobic part of a patterned surface than on the hydrophilic part.<sup>54</sup> If a surface changes its hydrophilicity/hydrophobicity during a sonochemical process, it is clear that the sponge response to ultrasound becomes nonlinear. The presence of additives in the sonochemical reactor can also influence the cavitation process. The role of an additive can be played by monomer or polymer molecules (here pyrrole and polypyrrole, respectively). These additives accumulate at the gas–liquid interface of cavitation microbubbles and the formed 3-D network. During collapse, the center of the bubble is characterised by high temperatures and pressures, whereas the bulk liquid remains under normal conditions. A transition zone also exists between the interface and bulk liquid.<sup>55</sup> Molecules are present in both the transition zone and the outer liquid phase. Additives or formed species (Fig. 3) can even penetrate inside bubbles. Single-bubble sonoluminescence studies (Fig. 4) show that pyrrole present in the solution completely quenches the luminescence which means formed species are present and liable to react inside the bubble core. However, as can also be seen in Fig. 4, the presence of pyrrole at the interface does not affect the time of bubble collapse or the size of the bubble, which is related to the intensity of the scattered light.

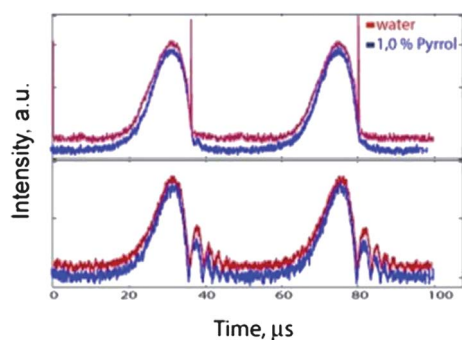


**Fig. 4** Time-resolved observation of single bubble collapse in pure water (upper curves, red) or pyrrole (lower curves, blue) containing solution. The sonoluminescence is superimposed on the scattered light signal at high acoustic pressure for water. In the presence of pyrrole this is completely quenched.

During the process of polymerisation the formation of long-chain molecules (polypyrrole) and the reactive species formed from them, such as long-chain radicals, takes place. The time required for the orientation of long-chain molecules at the gas–liquid interface is longer than that required for short-chain molecules and longer than the bubble lifetime.<sup>56</sup> The organic molecules, nanoparticles and ions near the bubble interface influence the cavitation process, which increases surface pressure, and leaves the molecules in the correct orientation and chemical state for transport and attachment to the surface.<sup>57</sup> Five main effects of cavitation are known for monomers and polymers: the formation of free radicals during the cavitation process,<sup>58</sup> polymerisation,<sup>59</sup> chain reorientation,<sup>60</sup> polymer decomposition<sup>61</sup> and the involvement of organics in chemical processes such as oxidation and bond breakage.<sup>62</sup>

Different hybrids can therefore be expected to form in our system. In particular, we found two main products (Figs. 3 and 5) depending on the solvents used: (1) interpenetrated magnesium polypyrrole (Mg–Ppy) hybrid formed in aqueous solution; (2) core@shell (Mg@Ppy) hybrid formed in alcohol solution. The presence of polypyrrole is visible in the FTIR spectra (Figs. 5e and f).<sup>63</sup> The peaks at 1540 and 1450  $\text{cm}^{-1}$  can be attributed to C–N and C–C asymmetric and symmetric ring-stretching, respectively. Additionally, the peaks near 1160 and 890  $\text{cm}^{-1}$  represent the doping state of polypyrrole, the peak at 1030  $\text{cm}^{-1}$  is attributed to C–H deformation and N–H stretching vibrations, and the broad band at 1300  $\text{cm}^{-1}$  is attributed to the C–H and C–N in-plane deformation vibrations, respectively. It is seen in the SEM and TEM images (Figs. 5a and c) that Mg–Ppy can still be characterised as porous with a rough surface. In alcohol solution a thicker amorphous (also see XRD pattern Fig. 5f) surface layer of polypyrrole Mg@Ppy with defined surface “flower” morphology is also observed (Figs. 5b and d). Differences in the structures formed could be due to differences in bubble collapse scenarios depending on the solution vapour pressure.<sup>64</sup> XRD and FTIR patterns (Fig. 5e and f) also provide evidence that oxidation in the presence of pyrrole in the solution proceeds more slowly in comparison with pure solution. Oxidation is slower since, first of all, the formed active oxygen species are involved in pyrrole polymerisation, which is apparent to the eye as a black color in solution.

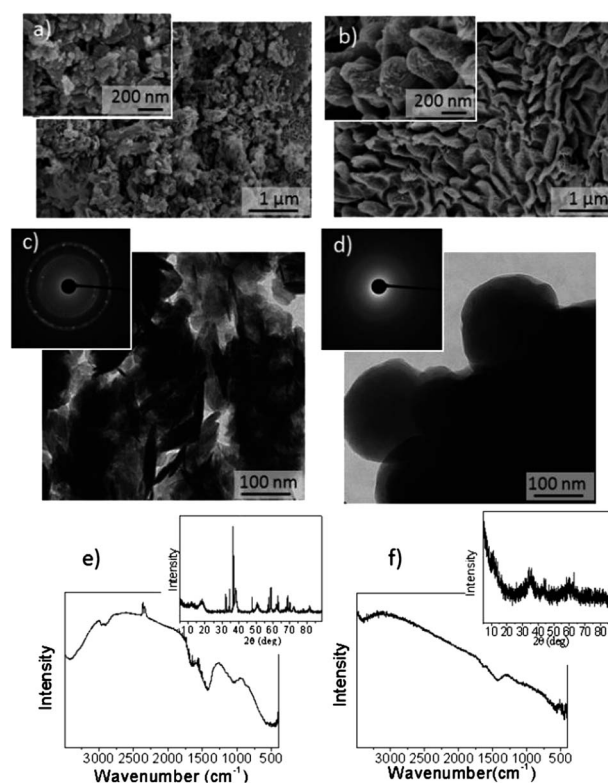


**Fig. 5** (a and b) SEM images, (c and d) TEM and ED (insets) images, (e and f) FTIR spectra and XRD patterns (insets) of structures formed after sonication (30 minutes) of magnesium in (a, c and e) aqueous or (b, d and f) methanol solution containing 5 wt% of pyrrole (monomer).

The process of polymerisation can be stimulated by initiators. Here we use Fe(III) as a known effective initiator for pyrrole polymerisation. However, if Fe(III) salt is added to the reaction medium together with the monomer, polymerisation starts very fast in solution and the formation of a pronounced 3-D network is difficult to achieve. We performed short-time pre-sonication of our  $\mu$ -sized magnesium particles in Fe(III) solution to achieve the formation of the first level of a 3-D network containing the initiation centers inside the 3-D network. Pyrrole solution was subsequently added as the second step in the 3-D network formation/modification. It is seen in the optical image (Fig. 6a, inset) that the resulting hybrid also exhibits the pronounced characteristic polypyrrole black color. FTIR spectra (Fig. 6c) reveal the characteristic polypyrrole bands, which are narrower in comparison with the previous case of hybrid formation without initiator. There was no evidence of interconnectivity between the formed polypyrrole (see TEM image in Fig. 6b). The polypyrrole formed is localised in the pores of magnesium. This result can be explained by taking into account the faster polymerisation with initiator and the negligible time for rearrangement of the polymer structure especially when the polymer is inside the porous magnesium and not in the solution. Such hybrids with formed polymer of lower molecular weight could potentially be used in the future for some interesting purposes, such as for the second rearrangement of the polymer structure. However, it is the interpenetrating hybrid, as for Mg–Ppy formed without initiator, that is of the greatest interest here because of its possible multi-trigger (pH and electric current flow active

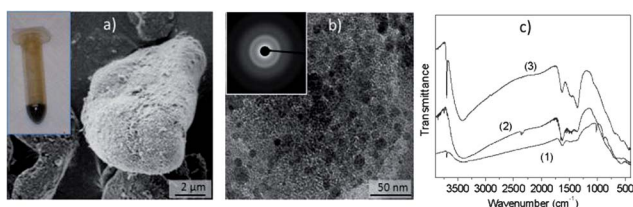


**Fig. 6** (a) SEM and sample tube optical (inset) images, (b) TEM and ED (inset) images of a magnesium-polypyrrole hybrid formed after the sonication (30 minutes) of Fe(III) (initiator of polymerisation)-loaded magnesium in aqueous solution containing 5 wt% of pyrrole (monomer). (c) FTIR spectra of the hybrids formed after sonication with varying concentration of magnesium particles in solution: (1) 0.3 g mL<sup>-1</sup>, (2) 0.05 g mL<sup>-1</sup>, (3) 0.1 g mL<sup>-1</sup>.

chemical release) capability. Before beginning our study it was assumed that magnesium would be responsible for pH-triggered release due to its chemical properties. Ppy was expected to be responsible for electrically stimulated release if the formation of a connected network through the entire hybrid could be achieved.

Here a single-step loading of Mg-Ppy hybrid carriers (capsules) with Rh6G by ultrasonic treatment of a Rh6G solution<sup>23</sup> (Fig. 7) was established. The multi-step loading, as reported in our previous work,<sup>65-67</sup> of a pre-formed magnesium 3-D network applying vacuum pump loading is possible. However, it goes without saying that a single-step process is economically preferable in materials synthesis. Using a single-step approach, we then continued sonication with pyrrole in solution for the formation of interpenetrating Mg-Ppy-Rh6G hybrids. The confocal fluorescence and SEM images of the

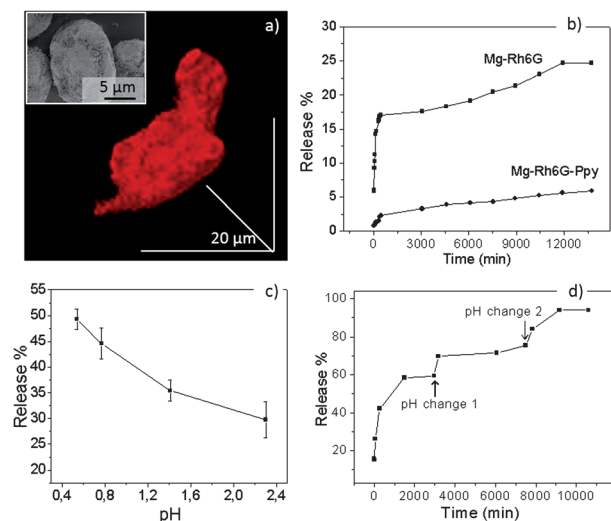


**Fig. 7** (a) 3-D confocal microscopy reconstruction of the sonona-engineered magnesium-polypyrrole hybrid loaded with fluorophore Rhodamin 6G (Rh6G) (fluorescence mode); the inset shows the SEM image of the hybrid. (b) Time-resolved release of Rh6G from porous magnesium (Mg-Rh6G) and the hybrid capsules (Mg-Rh6G-Ppy) in aqueous solution at neutral pH. (c) Rh6G release after 60 minutes in aqueous solution at different acidic pH values. (d) Time-resolved release under initial pH = 4 and two step-wise pH changes: pH change 1 to pH = 3 and pH change 2 to pH = 1.

formed structure are shown in Fig. 7a; it is seen that Rh6G can be stored in such a hybrid. Rh6G loading contents were 0.05 g g<sup>-1</sup> and 0.03 g g<sup>-1</sup> in the case of Mg-Rh6G and Mg-Ppy-Rh6G, respectively. In our previous work (ref. 23) the possibility was discussed of loading due to chemisorption; however, here there was no chemisorption detected, and thus the loading is due to physical Rh6G entrapment. From the release kinetics (Fig. 7b), it can also be seen that a hybrid Mg-Ppy carrier has better long-term storage ability in comparison with magnesium loaded with Rh6G. Thus, Ppy can prevent the fast degradation of magnesium in aqueous solution as could be the case for unprotected magnesium. However, from the perspective of implant construction, both systems could be promising for drug, vitamin, antibody and protein delivery. It is also very important that the pH dramatically affects Rh6G release. The release kinetics after an hour from Mg-Ppy-Rh6G at different pH values are shown in Fig. 7c. Moreover, the step-wise release is also characteristic of such hybrids (Fig. 7d).

One of the advantages of polypyrrole is its conductive nature, a characteristic which it imparts to the hybrids presented here, namely Mg-Ppy-Rh6G. The formation of nickel patterns on ITO glass (Fig. 8b) was performed, as described in our previous work (ref. 38-40). We used the sonoimpregnation procedure (Fig. 8a) for the deposition of Mg-Ppy-Rh6G hybrids onto a nickel metal surface. In this way, the sonication of ITO glasses in the presence of loaded hybrids can result in the connection of the hybrids with nickel occurring much faster than a possible connection of the hybrid with ITO glass.<sup>68</sup> The melting

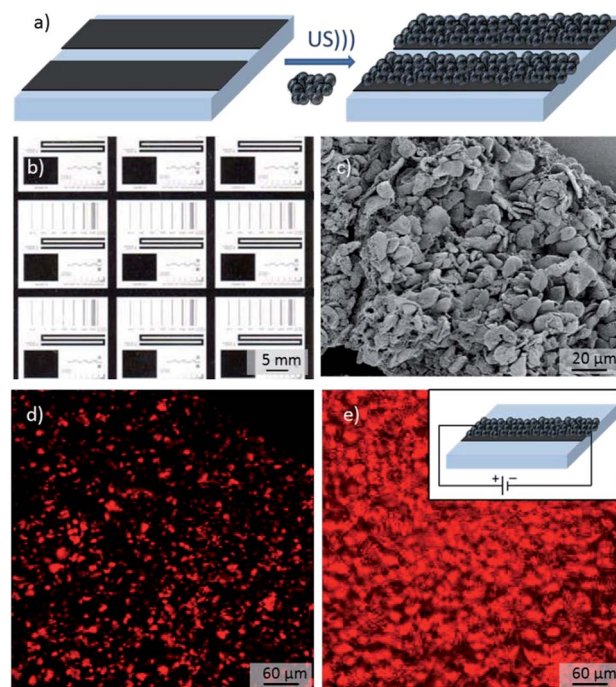


**Fig. 8** (a) Schematic representation of the process of sonoimpregnation (5 minutes) of hybrid particles on a patterned surface. (b) Optical image of the initial nickel patterned ITO glass electrode. (c) SEM image of patterned sonoimpregnated surface of Rh6G-loaded hybrid. (d) Confocal microscopy image (fluorescent mode) of (c). (e) (d) after electric current flow (shown schematically in the inset).

temperatures of the substrate (the part of the substrate with the metal patterns) and the hybrid, as well as the time of sonication, are critical parameters for this study. Since we use short-term sonication, we prevent the sonoimpregnation of the loaded hybrid into ITO glass, evident in the SEM image (Fig. 8c). The electric current in such a system as depicted schematically in Fig. 8e (inset) results in the release of Rh6G from the hybrid due to a change in polymer density. This can be seen in the confocal fluorescence images of a surface with sonoimmobilised capsules before and after electrical current (Figs. 8d and e, respectively).

## Conclusions

Effective hybrid capsules with synergetic trigger release are expected to be of great interest for the next decade, since time- and space-resolved release of active chemicals (labelling fluorescent dyes, drugs, vitamins, antibodies, etc.) could provide further successful use of encapsulation systems in the construction of medical devices, corrosion termination and as surfaces for stem cell research. We presented here a solution of the problem. Thus, hybrid systems whose components are sensitive to different factors (such as Mg to pH change, and polypyrrole to electric current flow) represent ideal candidates in the design of such capsules. We have presented a sonochemical approach for the formation of such hybrids, which has great potential due to its ecologically friendly nature and amount of process steps, additives and reagents.

## Acknowledgements

This work was supported by the Humboldt Foundation, SFB840, NATO CLG 984267 and FP7-NMP-2009-4.0-3-245572 3MICRON.

## Notes and references

- 1 *Handbook of Organic Conductive Molecules and Polymers*, ed. H. S. Nalwa, John Wiley & Sons, New York, 1997.
- 2 D. E. Tallman, G. Spinks, A. Dominis and G. G. Wallace, *J. Solid State Electrochem.*, 2002, **6**, 73.
- 3 E. V. Skorb and D. G. Shchukin, in *European Coatings Tech Files*, ed. G. Gehrenkemper, Vincentz Network GmbH & Co, Germany, 2010.
- 4 M. Gerard, A. Chaubey and B. D. Malhotra, *Biosens. Bioelectron.*, 2002, **17**, 345.
- 5 N. K. Guimard, N. Gomez and C. E. Schmidt, *Prog. Polym. Sci.*, 2007, **32**, 876.
- 6 J. Janata and M. Josowicz, *Nat. Mater.*, 2003, **2**, 19.
- 7 J.-D. Kwon, P.-H. Kim, J.-H. Keum and J. S. Kim, *Sol. Energy Mater. Sol. Cells*, 2004, **83**, 311.
- 8 R. Bashyam and P. Zelenay, *Nature*, 2006, **443**, 63.
- 9 T. Mirfakhraei, J. D. W. Madden and R. H. Baughman, *Mater. Today*, 2007, **10**, 30.
- 10 D. V. Andreeva, D. V. N. V. Bobrova, V. K. Lavrentév, Z. Pientka, G. A. Polotskaya and G. K. Elyashevich, *Polymer Sci. A.*, 2002, **44**, 424.
- 11 P. Mavinakuli, S. Wei, Q. Wang, A. B. Karki, S. Dhage, Z. Wang, D. P. Young and Z. Guo, *J. Phys. Chem. C*, 2010, **114**, 3874.
- 12 *New Concepts in Polymer Science*, ed. V. E. Gul', Brill Academic Pub., 1996.
- 13 D. V. Andreeva, D. A. Gorin, D. G. Shchukin and G. B. Sukhorukov, *Macromol. Rapid Commun.*, 2006, **27**, 931.
- 14 P. Gomez-Romero, *Adv. Mater.*, 2001, **13**, 163.
- 15 A. Malinauskas, J. Malinauskiene and A. Ramanavicius, *Nanotechnology*, 2005, **16**, R51.
- 16 M. P. Staiger, A. M. Pietak, J. Huadmaia and G. Dias, *Biomaterials*, 2006, **27**, 1728.
- 17 F. Witte, V. Kaese, H. Haferkamp, E. Switzer, A. Meyer-Lindenberg, C. J. Wirth and H. Windhagen, *Biomaterials*, 2005, **26**, 3557.
- 18 D. V. Volodkin, R. Klitzing and H. Möhwald, *Angew. Chem., Int. Ed.*, 2010, **49**, 9258.
- 19 K. S. Suslick and L. A. Crum, *Encyclopedia of Acoustics*, ed. M. J. Crocker, Wiley & Sons, Inc., N.Y., 1995.
- 20 M. A. Margulis, in *Sonochemistry Basis*, High School, Moscow, 1984.
- 21 E. V. Skorb, D. Fix, D. G. Shchukin, H. Möhwald, D. V. Sviridov, R. Mousa, N. Wanderka, J. Schäferhans, N. Pazos-Pérez, A. Fery and D. V. Andreeva, *Nanoscale*, 2011, **3**, 985.
- 22 D. G. Shchukin, E. V. Skorb, V. Belova and H. Möhwald, *Adv. Mater.*, 2011, **23**, 1922.
- 23 D. V. Andreeva, D. V. Sviridov, A. Masic, H. Möhwald and E. V. Skorb, *Small*, 2012, **8**, 820.
- 24 F. G. Hammitt, in *Cavitation and Multiphase Flow Phenomena*, McGraw-Hill Book Co., N.Y., 1980.
- 25 M. Stamm, *Polymer Surfaces and Interfaces*, Springer, Berlin, 2008.
- 26 D. G. Shchukin, D. V. Andreeva, E. V. Skorb and H. Möhwald, in *Supramolecular Chemistry of Hybrid Materials*, ed. K. Rurack, Wiley-VCH, Germany, 2010.
- 27 D. V. Andreeva, E. V. Skorb and D. G. Shchukin, *ACS Appl. Mater. Interfaces*, 2010, **2**, 1954.
- 28 L. J. Gerenser and K. E. Goppert-Berarducci, in *Metallized Plastics, Fundamental and Applied Aspects*, ed. K. L. Mittal, Plenum Press, N.Y., 1992.
- 29 M. Rubinstein and R. H. Colby, *Polymer Physics*, Oxford University Press Inc., N.Y., 2003.
- 30 G. Ferey, Hybrid porous solids: past, present, future, *Chem. Soc. Rev.*, 2008, **37**, 191.
- 31 *Dye Laser Principles*, ed. F. Duarte and L. Hillman, Academic, N.Y., 1990.
- 32 J.-H. Wang, J. Bartlett, A. Dunn, S. Small, S. Willis, M. Driver and A. Lewis, *J. Microsc.*, 2005, **217**, 216.
- 33 J. Gensel, T. Borke, N. Pazos-Pérez, A. Fery, E. Betthausen, A. H. E. Müller, D. V. Andreeva, H. Möhwald and E. V. Skorb, *Adv. Mater.*, 2012, **24**, 985.
- 34 K. Kellar and M. Iannone, *Exp. Hematol.*, 2002, **30**, 1227.
- 35 G. Visscher, M. Haseldonckx, W. Flameng, M. Borgers, R. Reneman and K. Rossem, *J. Neurosci. Methods*, 2003, **122**, 149.
- 36 D. Yu, J. An, J. Bae, D. Jung, S. Kim, S. Ahn, S. Kang and K. Suh, *Chem. Mater.*, 2004, **16**, 4693.
- 37 D. V. Andreeva, Z. Pientka, L. Brozová, M. Bleha, G. A. Polotskaya and G. K. Elyashevich, *Thin Solid Films*, 2002, **406**, 54.
- 38 E. V. Skorb, T. V. Byk, V. G. Sokolov, T. V. Gaevskaya, D. V. Sviridov, C.-H. Noh, K. Y. Song, Y. N. Kwon and S. H. Cho, *J. Photochem. Photobiol., A*, 2008, **193**, 56.
- 39 E. V. Skorb, T. V. Byk, V. G. Sokolov, T. V. Gaevskaya, D. V. Sviridov and C.-H. Noh, *High Energy Chem.*, 2008, **42**, 127.
- 40 E. V. Skorb, T. V. Byk, V. G. Sokolov, T. V. Gaevskaya and D. V. Sviridov, *Theor. Exp. Chem.*, 2009, **45**, 40.
- 41 T. Matula, *Philos. Trans. R. Soc. London, Ser. A*, 1999, **357**, 225.
- 42 *Emerging Technologies and Techniques in Porous Media*, ed. D. B. Ingham, Springer, 2004, p. 507.
- 43 *Porous Media: Applications in Biological Systems and Biotechnology*, ed. K. Vafai, CRC Press, 2010, p. 599.
- 44 J.-R. Li, R. J. Kuppler and H.-C. Zhou, *Chem. Soc. Rev.*, 2009, **38**, 1477.
- 45 E. V. Skorb, H. Möhwald, T. Irrgang, A. Fery and D. V. Andreeva, *Chem. Commun.*, 2010, **46**, 7897.
- 46 E. V. Skorb, D. G. Shchukin, H. Möhwald and D. V. Andreeva, *Nanoscale*, 2010, **2**, 722.
- 47 N. Pazos-Pérez, J. Schäferhans, E. V. Skorb, A. Fery and D. V. Andreeva, *Microporous Mesoporous Mater.*, 2012, **154**, 164.
- 48 J. Schäferhans, S. Gómez-Quero, D. V. Andreeva and G. Rothenberg, *Chem.-Eur. J.*, 2011, **17**, 12254.
- 49 V. P. Skripov, E. N. Sinitsyn, P. A. Pavlov, O. V. Ermakov, G. N. Muratov, N. V. Bulanov and V. G. Baidakov, *Thermophysical Properties of Liquids in the Metastable (Superheated) State*, Gordon and Breach, N.Y., 1988.
- 50 E. A. Neppiras, *Phys. Rep.*, 1980, **61**, 160.
- 51 K. S. Suslick and G. J. Price, *Annu. Rev. Mater. Sci.*, 1999, **29**, 295.
- 52 J. G. Adewuyi, *Environ. Sci. Technol.*, 2005, **39**, 8557.
- 53 J. Z. Sostarcic and P. Riesz, *J. Phys. Chem. B*, 2002, **106**, 12537.
- 54 V. Belova, D. A. Gorin, D. G. Shchukin and H. Möhwald, *Angew. Chem., Int. Ed.*, 2010, **49**, 7129.
- 55 D. G. Shchukin and H. Möhwald, *Phys. Chem. Chem. Phys.*, 2006, **8**, 3496.

- 56 J. Z. Sostaric and P. Riesz, *J. Am. Chem. Soc.*, 2001, **123**, 11010.
- 57 L. H. Thompson and L. K. Doraiswamy, *Ind. Eng. Chem. Res.*, 1999, **38**, 1215.
- 58 H. Endo, *J. Acoust. Soc. Am.*, 1994, **95**, 2409.
- 59 M. Zeng, H. N. Gao, Z. Q. Wu, L. R. Fan, T. H. Zheng and D. F. Zhou, *J. Macromol. Sci., Part A: Pure Appl. Chem.*, 2010, **47**, 1042.
- 60 A. V. Mohod and P. R. Gogate, *Ultrason. Sonochem.*, 2011, **18**, 727.
- 61 M. M. Caruso, D. A. Davis, Q. Shen, S. A. Odom, N. R. Sottos, S. R. White and J. S. Moore, *Chem. Rev.*, 2009, **109**, 5755.
- 62 K. Okitsu, Y. Mizukoshi, H. Bandow, T. A. Yamamoto, Y. Nagata and Y. Maeda, *J. Phys. Chem. B*, 1997, **101**, 5470.
- 63 M. Omastova, M. Trchova, J. Kovarova and J. Stejskal, *Synth. Met.*, 2003, **138**, 447.
- 64 D. J. Flannigan, S. D. Hopkins and K. S. Suslick, *J. Organomet. Chem.*, 2005, **690**, 3513.
- 65 E. V. Skorb, D. Fix, D. V. Andreeva, D. G. Shchukin and H. Möhwald, *Adv. Funct. Mater.*, 2009, **19**, 2373.
- 66 E. V. Skorb, D. G. Shchukin, H. Möhwald and D. V. Sviridov, *J. Mater. Chem.*, 2009, **19**, 4931.
- 67 E. V. Skorb, D. V. Sviridov, H. Möhwald and D. G. Shchukin, *Chem. Commun.*, 2009, 6041.
- 68 M. Viot, T. Chave, S. I. Nikitenko, D. G. Shchukin, T. Zemb and H. Möhwald, *J. Phys. Chem. C*, 2010, **114**, 13083.